



CDF note 8942

## Direct Measurement of $W$ Boson Charge Asymmetry with $1 \text{ fb}^{-1}$ of Run II Data

The CDF Collaboration  
URL <http://www-cdf.fnal.gov>  
(Dated: August 4, 2007)

We present a new analysis method which directly reconstructs the  $W$  rapidity from  $W \rightarrow e\nu$  data to measure the  $W$  boson charge asymmetry in  $p\bar{p}$  collisions at  $\sqrt{s} = 1.96 \text{ TeV}$  using an integrated luminosity of  $1 \text{ fb}^{-1}$ . The asymmetry provides new input on the momentum fraction dependence of the  $u$  and  $d$  quark parton distribution functions (PDF) within the proton.

*Preliminary Results for Lepton-Photon 2007 Conferences*

## I. INTRODUCTION

$W^+(W^-)$  bosons are produced in  $p\bar{p}$  collisions primarily by the annihilation of  $u(d)$  quarks from the proton and  $\bar{d}(\bar{u})$  quarks from the anti-proton. As the  $u$  quark tends to carry a higher fraction of the proton's momentum than the  $d$  quark, the  $W^+(W^-)$  is boosted, on average, in the proton (anti-proton) direction as shown in Figure 1.

The  $W^\pm$  charge asymmetry is defined as

$$A(y_W) = \frac{d\sigma(W^+)/dy_W - d\sigma(W^-)/dy_W}{d\sigma(W^+)/dy_W + d\sigma(W^-)/dy_W}, \quad (1)$$

where the subscript(+,-) denotes the charge of the  $W$  and  $y_W$  is the rapidity of the  $W$  bosons [1]. For  $p\bar{p}$  collisions in leading-order parton model,  $A(y_W)$  is given approximately by

$$A(y_W) \approx \frac{u(x_1)d(x_2) - d(x_1)u(x_2)}{u(x_1)d(x_2) + d(x_1)u(x_2)}, \quad (2)$$

where  $x_{1,2} = x_0 e^{\pm y_W}$  and  $x_0 = M_W/\sqrt{s}$ . A precise measurement of the  $W$  asymmetry is a sensitive probe of the momentum fraction difference between  $u$  and  $d$  quarks in the  $Q^2 \approx M_W^2$  region and is one of the best determinations of the proton  $d/u$  momentum ratio as a function of  $x$ , and plays an important role in global fits.

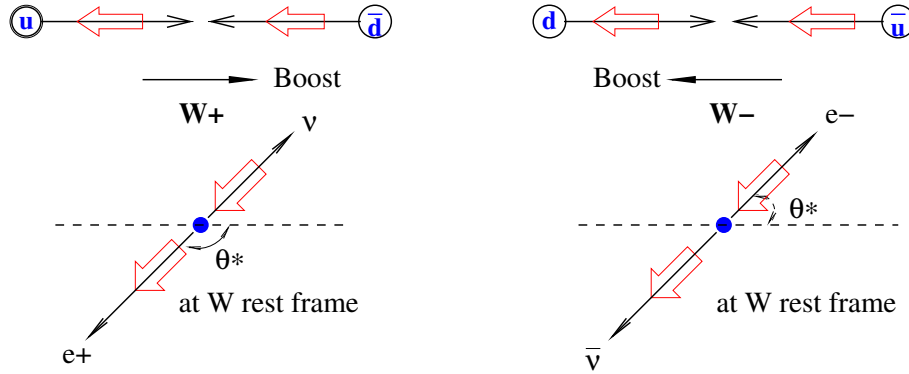


FIG. 1: The momenta (arrows) and helicities (large outlines of arrows) in  $p\bar{p} \rightarrow W^\pm$  production and  $W^\pm$  leptonic decay in leading order.

The  $W$  decay, in our case  $W^\pm \rightarrow e^\pm \nu$ , provides a high purity sample for measuring this asymmetry. But since the  $p_z$  of the neutrino is unmeasured, the asymmetry has been measured traditionally [2] [3] as

$$A(\eta_e) = \frac{d\sigma(e^+)/d\eta_e - d\sigma(e^-)/d\eta_e}{d\sigma(e^+)/d\eta_e + d\sigma(e^-)/d\eta_e}, \quad (3)$$

where  $\eta_e$  is the electron pseudo-rapidity. By assuming that the  $W \rightarrow e\nu$  decays are described by the Standard Model  $V-A$  (vector-axial vector) couplings, the electron asymmetry,  $A(\eta_e)$ , is a convolution of  $W^\pm$  production and decay asymmetries, which results in a change in sign of  $A(\eta_e)$  at high  $|\eta_e|$ . The predicted  $A(y_W)$  and  $A(\eta_e)$  are shown in Figure 2. However, we can determine the neutrino momentum up to a two-fold ambiguity by constraining the  $W$  mass. This ambiguity can be partly resolved on a statistical basis from the known  $V-A$  decay distribution for the center-of-mass decay angle  $\theta^*$  and of the  $W^\pm$  production cross-sections as a function of  $y_W$ ,  $d\sigma/dy$ .

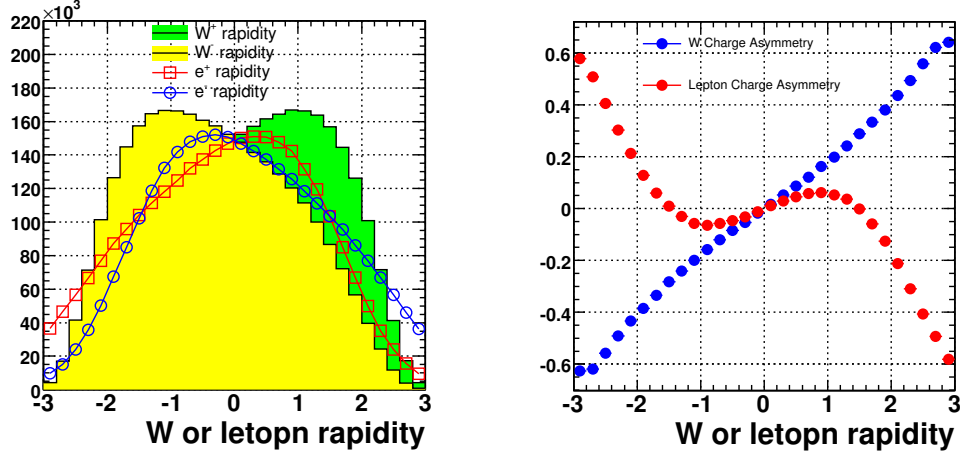


FIG. 2: The  $W$  boson and lepton rapidity distributions in  $p\bar{p}$  collisions (left) and the relationship between the  $W$  production charge asymmetry and lepton charge asymmetry from the  $W$  leptonic decay as a function of rapidity (right).

We use the Monte Carlo to estimate the production probability of the two factors. First, in Figure 3 we verify the expected angular distribution of  $(1 \pm \cos\theta)^2$  from the production of  $W^\pm$  with quarks in the proton and the opposite distribution with anti-quarks in the proton. The ratio of quark (proton) induced to anti-quark (proton) induced  $W$  production therefore determines the angular decay distribution. In the simulation, we measure the fraction of each, and parameterize the angular distributions as a function of  $y_W$  and the  $W$  transverse momentum,  $P_T^W$ . We find the functional form:

$$P_\pm(\cos\theta^*, y_W, P_T^W) = (1 \mp \cos\theta^*)^2 + Q(y_W, P_T^W)(1 \pm \cos\theta^*)^2, \quad (4)$$

$$Q(y_W, P_T^W) = f(P_T^W) e^{-[g(P_T^W) * y_W^2 + 0.05 * |y_W|^3]}, \quad (5)$$

$$f(P_T^W) = 0.2811 * \mathcal{L}(P_T^W, 21.7, 9.458) + 0.2185 * e^{(-0.04433 * P_T^W)} \quad (6)$$

$$g(P_T^W) = 0.2085 + 0.0074 * P_T^W - 5.051e^{-5} * P_T^{W^2} + 1.180e^{-7} * P_T^{W^3} \quad (7)$$

where  $\mathcal{L}(x, \mu, \sigma)$  is the Landau distribution with most probable value  $\mu$  and the RMS  $\sigma$ . The first term of Eqn. 4 corresponds to contributions from quarks in the proton and the second term from anti-quarks in the proton. The parameterization in Eqn. 5,  $Q(y_W, P_T^W)$  is obtained using MC@NLO including NLO QCD prediction [4].

The second relevant factor is the sum of the  $W^+$  and  $W^-$  cross-sections as a function of  $y_W$ . As shown in Figure 2,  $W$  boson production decreases sharply beyond  $|y_W| > 2$  because of the scarcity of high  $x$  quarks. Therefore, if two solutions are possible, one in the central region and another with  $|y_W| > 2$ , the former should receive more weight as the latter is very unlikely to be produced.

Finally, the weighting factor for each rapidity solution is represented as

$$wt_{1,2}^\pm = \frac{P_\pm(\cos\theta_{1,2}^*, y_{1,2}, P_T^W) \sigma_\pm(y_{1,2})}{P_\pm(\cos\theta_1^*, y_1, P_T^W) \sigma_\pm(y_1) + P_\pm(\cos\theta_2^*, y_2, P_T^W) \sigma_\pm(y_2)}, \quad (8)$$

where the  $\pm$  signs indicate the  $W$  boson charge and indices of 1, 2 are for the two  $W$  rapidity solutions. In Eqn 8, the weighting factor depends primarily on the  $W^+$  and  $W^-$  cross-sections, but does have some weak dependence on the  $W$  charge asymmetry itself. Therefore, this method requires us to iterate the procedure to eliminate the dependence of the asymmetry on the weighting factor for our measurement.

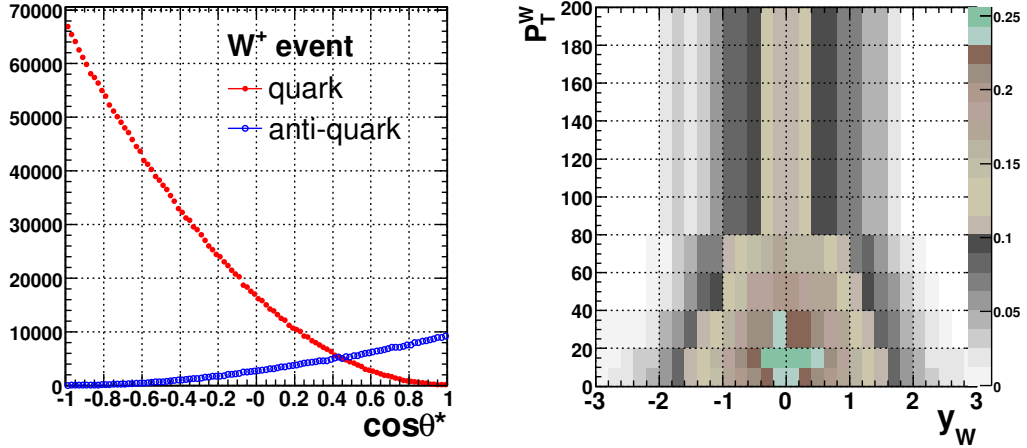


FIG. 3: The left plot shows the  $\cos\theta^*$  distributions of  $e^+$  in the  $W^+$  rest frame, averaged over all produced  $W$ . The labeled “quark” curve shows the case where a quark from the proton and an anti-quark from the anti-proton form the  $W$ , and “anti-quark” is the opposite case (i.e. an anti-quark from the proton and a quark from the anti-proton). The right plot shows the dependence of the ratio of “anti-quark” ( $\bar{q}$ ) and “quark” ( $q$ ) contributions to the overall  $W$  decay angle distribution as a function of  $W$  rapidity and  $p_T$  of the  $W$ .

## II. DATASET AND EVENT SELECTION

### A. Dataset

We use high- $p_T$  electron datasets in the central ( $|\eta_e| < 1$ ) and plug regions ( $1 < |\eta_e| < 2.8$ ), with an integrated luminosity of  $1 \text{ fb}^{-1}$ . All data runs used are required to pass our “good run” criteria for electrons with a working silicon detector. The following Monte Carlo samples are used to study the efficiencies of trigger and electron identification, the sensitivity of this new method and the systematics on the measurement of the  $W$  charge asymmetry. All Monte Carlo samples are generated with Pythia 6.216 (CTEQ5L), passed through the full simulation of the CDF detector and reconstructed.

- 19.8 million  $W \rightarrow e\nu$  events
- 10.1 million  $Z \rightarrow e^+e^-$  events
- 16.3 million  $W \rightarrow \tau\nu$  events

### B. Event Selection

The criteria used to identify the electron and positron candidates, summarized below, are designed to reject the energy deposits from photons or quark or gluon jets.

- $E_T > 25$  GeV for central electron and  $E_T > 20$  GeV for plug electron,
- $E_{Iso} < 4$ , where  $E_{Iso}$  is additional energy in an “isolation” cone with angular radius  $R = \sqrt{(\Delta\phi)^2 + (\Delta\eta)^2} = 0.4$  centered on the electron,
- A small amount of hadronic energy relative to the EM energy,
- Cuts on the shower shape in the EM calorimeter and shower maximum detector,
- A track consistent with the position and energy measured in the calorimeter

COT tracks, reconstructed independently of the calorimeter measurement, can be compared to it in position and momentum. However, the coverage of the COT is limited to  $|\eta_e| < 1.6$ . To extend the measurement to higher  $|\eta_e| < 2.8$ , silicon standalone tracks are reconstructed. The plug electrons are required to have a good quality track to identify the charge of the electron.

Candidate  $W \rightarrow e\nu$  events are required to have exactly one such  $e^\pm$  candidate as well as  $\cancel{E}_T > 25$  GeV. We found 537,858 events in central and 176,941 events in plug with this requirements.

### III. CORRECTIONS

In order to reconstruct the  $W$  charge asymmetry, the method described above needs to be corrected to account for several effects. These include:

- MC electron energy scale and resolution tuning
- correction to the  $\cancel{E}_T$  in events where the transverse mass of the electron and the  $\cancel{E}_T$  exceeds  $M_W$
- correction for charge mis-identification in the central and plug tracking
- correction for the background
- correction for the effects of smearing and detector acceptance

We provide further detail below on the charge mis-identification, background and acceptance corrections.

#### A. Charge Mis-Identification

Good charge identification is crucial for the asymmetry measurement because the charge determines the sign of the weight factor,  $wt^\pm$  (see Eqn. 8), which corresponds to the number of  $W^\pm$  rapidity events. Therefore, charge misidentification of electrons changes the  $W$  charge asymmetry and the charge misidentification rate needs to be properly determined. We measure the charge fake rate using  $Z \rightarrow ee$  events and the charge fake rate is defined as

$$f_{mis}(\eta) = \frac{N_{wrong-sign}(\eta)}{N_{right-sign}(\eta) + N_{wrong-sign}(\eta)}, \quad (9)$$

where  $N_{wrong-sign}$  is the number of  $Z$  candidates where two electrons have the same sign, and  $N_{right-sign}$  is the number where they have the opposite sign.

First, we need to identify a clean sample of  $Z \rightarrow e^+e^-$  decays that we can use to study this charge misidentification. The  $ee$  invariant mass is required to be between 76 and 106 GeV/ $c^2$  for  $Z$ s with two central electrons (central-central) and between 81 and 101 GeV/ $c^2$  for  $Z$ s with one central and one plug electron (central-plug). We measure the charge fake rate from the selected  $Z$  candidates vs.  $\eta$  and we find the charge fake rate is highly dependent on  $\eta$ , as shown in Figure 4.

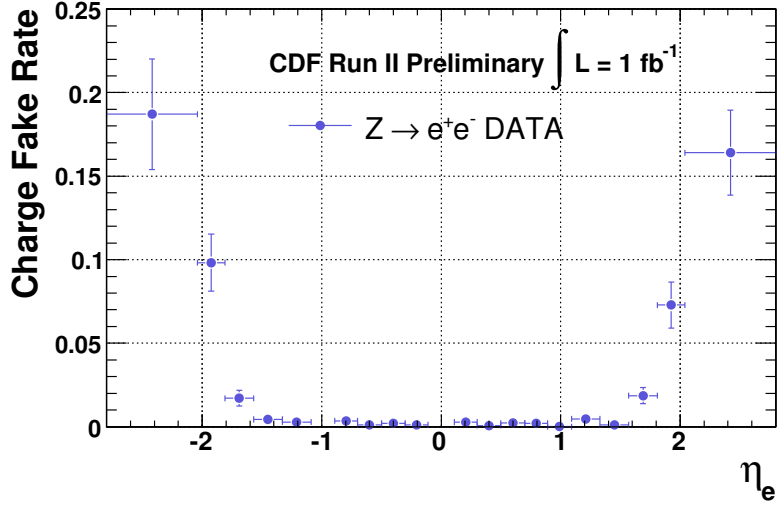


FIG. 4: The charge fake rate as a function of electron  $\eta$ .

In order to have a charge mis-identification correction for our asymmetry, we need to describe the charge fake rate as a function of  $W$  rapidity. Thus, we derive a correction of charge fake rate such that it can be put into the acceptance correction from the charge fake rate vs.  $\eta$  in Figure 4. We express the total reconstructed number of positively and negatively charged events in Eqn. 10 and the total number of true charged events in Eqn. 11, below.

$$\begin{aligned} N_{obs}^+(wt^+) &= N_+^+(wt^+) + N_+^-(wt^+) \\ N_{obs}^-(wt^-) &= N_-^-(wt^-) + N_-^+(wt^-) \end{aligned} \quad (10)$$

$$\begin{aligned} N_{true}^+ &= N_+^+(wt^+) + N_-^+(wt^+) \\ N_{true}^- &= N_-^-(wt^-) + N_+^-(wt^-) \end{aligned} \quad (11)$$

$N_+^-(wt^+)$  is the number of truly positive charge events reconstructed with a negative charge and is a function of the weight factor ( $wt$ ) in that bin of  $W$  rapidity. We then describe the number of true charged events with the reconstructed information and new factors in Eqn. 12 and 13, below.

$$\begin{aligned} N_{true}^+ &= [N_+^+(wt^+) + N_+^-(wt^+)] \times \frac{N_+^+(wt^+)}{[N_+^+(wt^+) + N_+^-(wt^+)]} \\ &\quad + [N_-^-(wt^+) + N_-^+(wt^+)] \times \frac{N_-^+(wt^+)}{[N_-^-(wt^+) + N_-^+(wt^+)]} \\ &= N_{obs}^+(wt^+) \times (1 - \rho^+(wt^+)) + N_{obs}^-(wt^+) \times (\rho^-(wt^+)) \end{aligned} \quad (12)$$

$$\begin{aligned} N_{true}^- &= [N_-^-(wt^-) + N_-^+(wt^-)] \times \frac{N_-^-(wt^-)}{[N_-^-(wt^-) + N_-^+(wt^-)]} \\ &\quad + [N_+^+(wt^-) + N_+^-(wt^-)] \times \frac{N_+^-(wt^-)}{[N_+^+(wt^-) + N_+^-(wt^-)]} \\ &= N_{obs}^-(wt^-) \times (1 - \rho^-(wt^-)) + N_{obs}^+(wt^-) \times (\rho^+(wt^-)) \end{aligned} \quad (13)$$

Therefore, we define the four charge fake rates in Eqn. 14, below, that are  $\rho^+(wt^+)$ ,  $\rho^+(wt^-)$ ,  $\rho^-(wt^-)$  and  $\rho^-(wt^+)$ , as the reconstructed charge and the weight factors of the two  $W$  rapidity solutions. However, since this correction depends on the  $W$  rapidity, it must be iterated for the measurement.

Since we know the electron pseudo-rapidity and the charge fake rate corresponding to the pseudo-rapidity per event, we can represent the four charge fake corrections with the measured charge fake rate in the  $\eta$  bin as shown in Figure 4.

$$\begin{aligned}
\rho^+(wt^+) &= \frac{N_+^-(wt^+)}{N_+^+(wt^+) + N_+^-(wt^+)} \\
\rho^+(wt^-) &= \frac{N_+^-(wt^-)}{N_+^+(wt^-) + N_+^-(wt^-)} \\
\rho^-(wt^-) &= \frac{N_-^+(wt^-)}{N_-^-(wt^-) + N_-^+(wt^-)} \\
\rho^-(wt^+) &= \frac{N_-^+(wt^+)}{N_-^-(wt^+) + N_-^+(wt^+)}
\end{aligned} \tag{14}$$

### B. Background correction

We apply corrections for two backgrounds: QCD and  $Z \rightarrow e^+e^-$ . Note that we consider the  $W \rightarrow \tau\nu \rightarrow e\nu$  as signal and it is included in the signal acceptance. For the  $Z \rightarrow e^+e^-$  background estimate, we rely on MC. However, for the QCD background estimate we use a technique for estimating the QCD background by fitting the isolation distribution of the electrons [5]. We fit the data to a signal template from  $Z \rightarrow e^+e^-$  data and a background template from dijet events in data. We also perform the fit separately for  $25 \text{ GeV} < \cancel{E}_T < 35 \text{ GeV}$  and  $35 \text{ GeV} < \cancel{E}_T < 200 \text{ GeV}$ . The background fractions we measure are summarized in Tables I and in Figure 5 QCD background rapidity distribution is shown as a function of  $y_W$ .

electron region $\cancel{E}_T$ region	central		plug	
	$25 < \cancel{E}_T < 35$	$35 < \cancel{E}_T < 200$	$25 < \cancel{E}_T < 35$	$35 < \cancel{E}_T < 200$
# of QCD	3216	3294	582	600
# of DATA	210592	327266	81528	95413
QCD fraction(%)	$1.527 \pm 0.117$	$1.007 \pm 0.084$	$0.713 \pm 0.087$	$0.628 \pm 0.079$
total fraction(%)	<b><math>1.210 \pm 0.144(\text{stat.}) \pm 0.146(\text{syst.})</math></b>		<b><math>0.668 \pm 0.117(\text{stat.}) \pm 0.143(\text{syst.})</math></b>	

TABLE I: QCD background fraction for central and plug electrons.

### C. Acceptance

The raw  $W$  charge asymmetry we measure must be corrected for detector acceptance and smearing effects to obtain the physical  $W$  asymmetry, which can be compared to theoretical calculations. We define a correction for the acceptance of kinematic cuts as a function of reconstructed  $y_W$ :

$$a^\pm(y_W) = \frac{\# \text{ of events from MC and simulation which pass cuts}}{\# \text{ of events from MC without cuts at generation level}}, \tag{15}$$

where the sign,  $\pm$ , indicates the charge of  $W$  boson. The acceptance depends on the charge of the  $W$  boson, and such effects need to be carefully studied and evaluated before being applied blindly in this

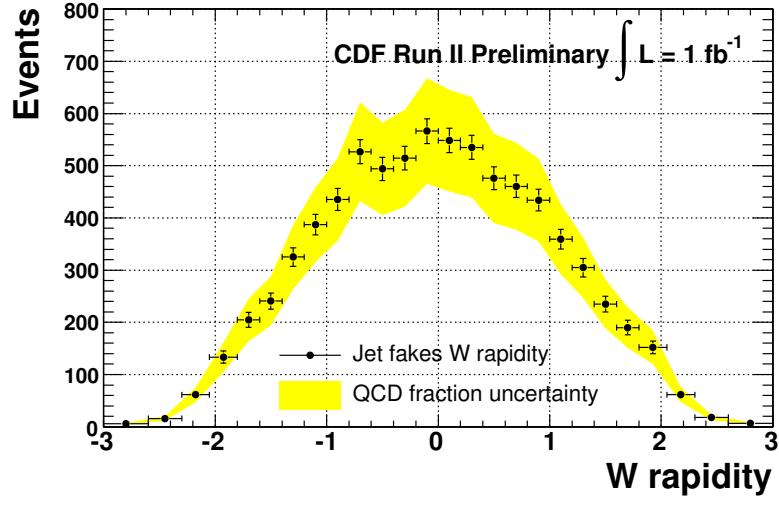


FIG. 5: QCD background rapidity distribution.

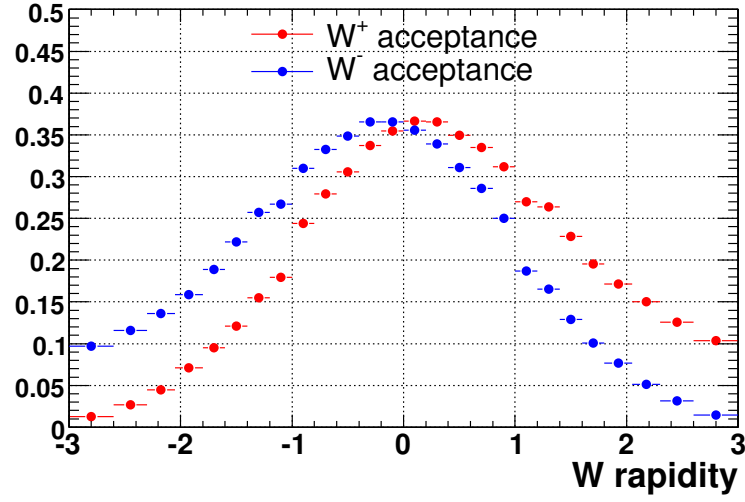


FIG. 6: The acceptance correction.

analysis because of their direct impact on the charge asymmetry. We also apply corrections to the acceptance to account for the trigger efficiency (which is not simulated) measured from the data, the electron ID efficiency scale factors (data/MC, i.e., correcting the MC to match the data) and the charge fake rate also measured in the data. The acceptance correction is shown in Figure 6.



	PDF	Et	Recoil	CFR	BKG	Trig	ID	Syst.	Stat.
$0 <  y_W  < 0.2$	0.00027	0.00014	0.0011	0.00017	0.00043	0.00029	0.00016	0.0013	0.0031
$0.2 <  y_W  < 0.4$	0.00077	0.00038	0.0022	0.00011	0.00091	0.0008	0.00067	0.0027	0.0032
$0.4 <  y_W  < 0.6$	0.0015	0.00055	0.0022	0.00018	0.0011	0.0013	0.0017	0.0037	0.0033
$0.6 <  y_W  < 0.8$	0.0022	0.00071	0.0034	0.00025	0.0015	0.0014	0.003	0.0055	0.0032
$0.8 <  y_W  < 1$	0.0024	0.00071	0.0042	0.00031	0.002	0.0011	0.0047	0.0072	0.0034
$1 <  y_W  < 1.2$	0.0027	0.00079	0.0033	0.0004	0.0018	0.00089	0.0069	0.0084	0.0038
$1.2 <  y_W  < 1.4$	0.0028	0.0015	0.0067	0.00047	0.0018	0.00059	0.0078	0.011	0.0043
$1.4 <  y_W  < 1.6$	0.0028	0.0014	0.011	0.00035	0.0014	0.0004	0.0085	0.014	0.005
$1.6 <  y_W  < 1.8$	0.0029	0.0026	0.0092	0.00077	0.0012	0.00028	0.0089	0.013	0.0055
$1.8 <  y_W  < 2$	0.0034	0.0031	0.0082	0.0022	0.0013	0.00056	0.008	0.013	0.0062
$2 <  y_W  < 2.3$	0.0042	0.0053	0.0059	0.0044	0.0021	0.0017	0.0085	0.013	0.0083
$2.3 <  y_W  < 2.6$	0.005	0.0062	0.004	0.0045	0.0019	0.0027	0.0086	0.014	0.011
$2.6 <  y_W  < 3$	0.0053	0.006	0.0043	0.0014	0.001	0.0028	0.0065	0.012	0.023

TABLE II: Uncertainty categories for the  $W$  production charge asymmetry. The uncertainties in higher  $W$  rapidity bins for each category are shown.

#### IV. SYSTEMATIC UNCERTAINTIES

We consider potentially significant sources of systematic uncertainty on the  $W$  charge asymmetry measurement. The uncertainties on the weighting factor given in Eqn 8 arise from uncertainties on the momentum distribution of quarks and gluons in the proton modeled with the PDF sets used. The choice of PDF set has an effect on the shape of the  $d\sigma^\pm/dy_W$  distributions as well as the ratio of quark and anti-quark in the angular decay distribution.

We use the CTEQ6 error PDF sets [6] and perform the  $d\sigma^\pm/dy_W$  production cross section and the angular distribution of  $(1 \pm \cos\theta^*)^2$  for each error PDF set. We determine the uncertainty on the  $W$  charge asymmetry by checking how much the asymmetry values based on each calculation deviate from the value obtained using the best-fit PDF set.

We also consider experimental sources of systematic uncertainty. The cluster  $E_T$  scale and resolution for electromagnetic sections of the calorimeter can change  $W$  rapidity and the asymmetry measurement. The asymmetry uncertainties are estimated as the changes in measured asymmetry for each candidate sample that occur when the cluster  $E_T$  is changed between its default and  $\pm\sigma$  value. To account for the effect of the missing  $E_T$  scale in our  $W \rightarrow e\nu$  sample, we consider the boson recoil energy (affected by multiple interactions) since an accurate model of the event recoil energy in the simulation is important for estimating the acceptance of the event  $\cancel{E}_T$ . The charge misidentification and backgrounds are crucial for the charge asymmetry measurement since both contributions can directly change our result.

In Table II, we summarize the systematic uncertainties of the the  $W$  boson charge asymmetry measurement and can be compares with the statistical uncertainty obtained in this  $1 \text{ fb}^{-1}$  measurement.

#### V. RESULTS

We present a direct measurement of the  $W$  production charge asymmetry using an integrated luminosity of  $1 \text{ fb}^{-1}$ . We use a new analysis method which directly reconstructs the  $W$  rapidity. We consider two possible  $W$  rapidity solutions because of the unknown longitudinal momentum of the neutrino from the  $W$  decay. We determine the relative contribution of the event to the two solutions according to the  $V - A$  decay structure of the weak interaction and the dependence of  $W$  boson rapidity upon the differential cross-section,  $d(\sigma_W)/dy$ .

Our results are summarized in Figure 7 and Figure 8 and show the corrected asymmetry as a function of  $y_W$ . We compare to an NNLO prediction [7] using MRST2002 PDFs [8] and find good agreement. In Figure 8 we also compare our result to the predicted  $W$  charge asymmetries of PDFs

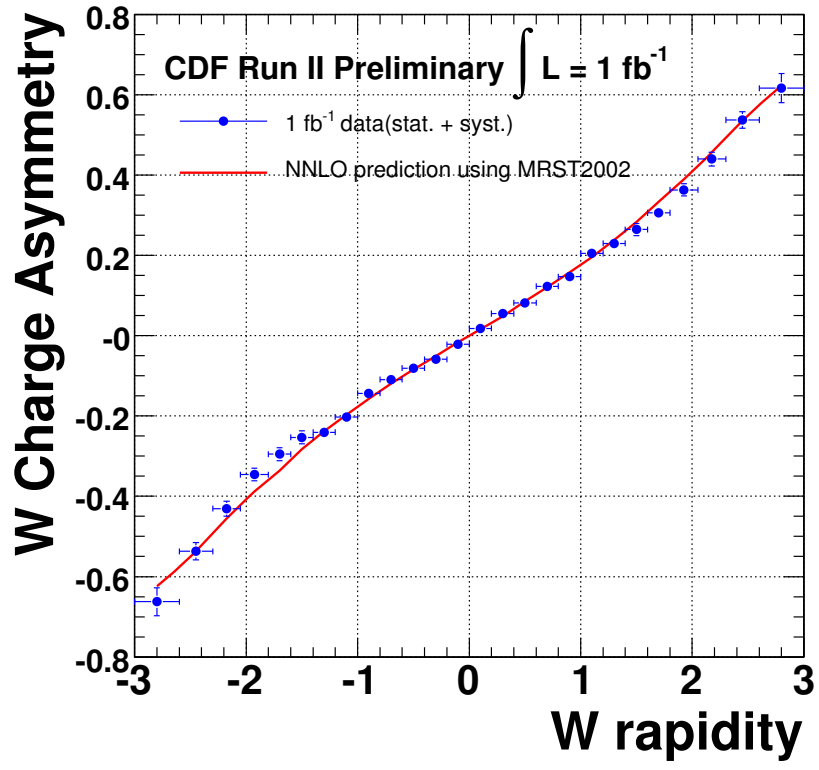


FIG. 7: The corrected  $W$  production charge asymmetry. The black error bars indicate the total uncertainty(stat.+ syst.) and the blue error bars represent the statistical uncertainty only.

using CTEQ5L and the corresponding error PDFs from CTEQ6.1 described by 20 parameters [6].

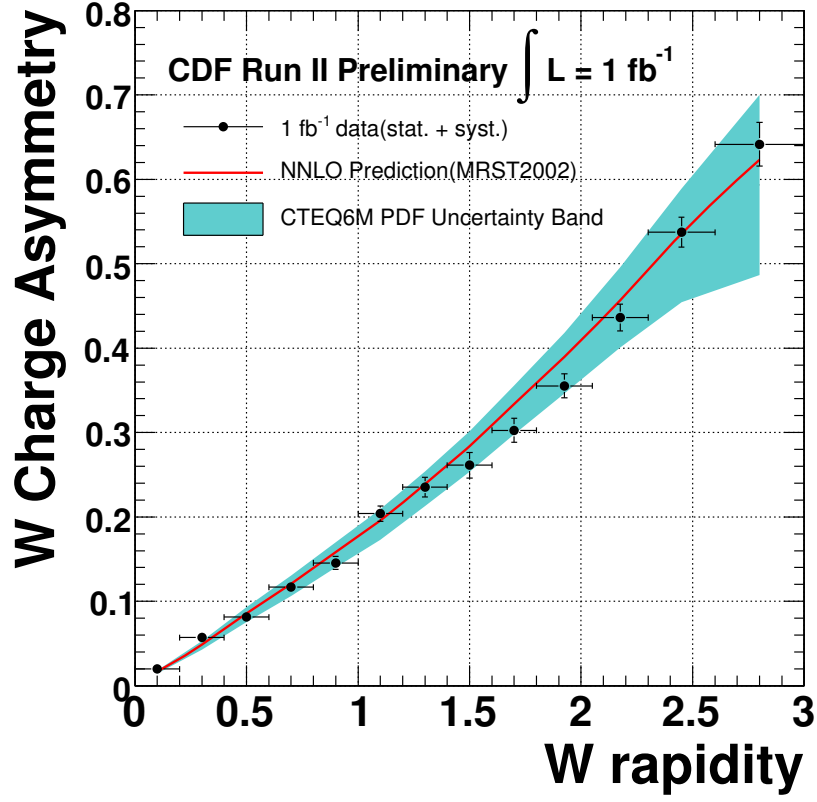


FIG. 8: The measured asymmetry,  $A(|y_W|)$ , is plotted and prediction from the CTEQ5L. The band curves are from the variation of 20 pairs of independent PDF parameters and illustrate the range of uncertainty on the CTEQ prediction.

- 
- [1] A.D. Martin *et al.*, *Phys. Rev. D* **50**(1994)6734.
  - [2] Qun Fan *et al.*, CDF Note 5566.
  - [3] D. Acosta *et al.*, *Phys. Rev. D* **71**(2005)051104.
  - [4] S. Frixione, P. Nason and B.R. Webber, Matching NLO QCD and parton showers in heavy flavour production, *J. High Energy Phys.***0308** (2003) 007, hep-ph/0305252.
  - [5] B-Y. Han *et al.*, "Backgrounds in  $W \rightarrow e\nu$  for the  $W$  Production Charge Asymmetry Analysis", CDF note 8196.
  - [6] J. Pumplin *et al.*, "New generation of parton distributions with uncertainties from global QCD analysis", hep-ph/0201195
  - [7] C. Anastasiou *et al.*, *Phys. Rev. D***69**, 094008 (2004)
  - [8] A. D. Martin *et al.*, *Eur. Phys. J.*, **C28**, 455 (2003)